Journal of the European Ceramic Society 22 (2002) 2297–2303
www.elsevier.com/locate/jeurceramsoc

Experimental study of the SnO_2–ZrO_2 phase diagram

B. Gaillard-Allemand, R. Podor*, M. Vilasi, Ch. Rapin, A. Maître, P. Steinmetz

Laboratoire de Chimie du Solide Minéral, UMR 7555, Université Henri Poincaré, Faculté des Sciences, BP 239, 54 506 Vandoeuvre-Lès-Nancy Cedex, France

Received 13 November 2001; received in revised form 13 February 2002; accepted 24 February 2002

Abstract

The study of the SnO_2–ZrO_2 phase diagram in the 1230–1750 °C temperature range has shown the existence of an immiscibility gap, leading to two $(Zr_{1-x}Sn_x)O_2$ and $(Sn_{1-y}Zr_y)O_2$ limited solid solutions. Four compositions were synthesised for each solid solution, leading to pure phases, which were characterised by room-temperature and high-temperature X-ray diffraction. The unit-cell parameters of tetragonal $(Sn_{1-y}Zr_y)O_2$, monoclinic $(Zr_{1-x}Sn_x)O_2$ and tetragonal $(Zr_{1-x}Sn_x)O_2$ were determined and correlated with the content of the substituted atom. The monoclinic to tetragonal and reverse reactions for the $(Zr_{1-x}Sn_x)O_2$ series were also characterised (transition temperatures) when varying the tin mole fraction.

Keywords: Phase diagram; SnO_2; Solid solution; Transition temperature; Unit-cell parameter; ZrO_2; SnO_2-ZrO_2

1. Introduction

In the course for the development of new fully densified ceramic materials for industrial applications, we have focused our attention on both ZrO_2 and SnO_2 based ceramics. These materials are already used for specific applications such as heating electrodes or oven bricks. Nevertheless, any corrosion of these materials in molten silicate slag is often observed. On the one hand, the interaction between molten slag and zirconia may lead to the formation of $ZrSiO_4$. On the other hand, commercially available SnO_2-based ceramics are prepared with a glass-bond which dissolves into the slag in contact with the pieces. This phenomena slowly yields to the material decohesion. Furthermore, the direct contact between SnO_2 and a metallic piece at temperature higher than 700 °C induces the oxidation of metal and reduction of SnO_2 into liquid tin according to Ellingham's diagram. The decomposition of SnO_2 into SnO[1,2] according to Eq. (1) cannot be neglected at temperature higher than 1300 °C.

$$SnO_2(s) \rightarrow SnO(g) + 1/2O_2(g) \quad (1)$$

The dilution of tin in SnO_2 by substitution of Sn with significant amounts of ZrO_2 may decrease the activity of Sn in the new compound. This will yield to a material which solubility in silicate liquids will be low, which will be less reactive with metals than pure SnO_2, which will not dissociate as easily as pure SnO_2 at high temperature and which melting point will be higher than 1630 °C (melting point for pure SnO_2).

The necessity to achieve compounds whose density is close to the theoretical one is inherent in the applications which are dedicated to these materials. Cerri et al.[3] have shown that the addition of 0.5 mol.% of CoO (or CuO[4,5]) as a sintering aid is enough to improve the densification of SnO_2 ceramics by forming lattice solid solution. In our work, 0.5 mol% of CoO have always been added to the materials we have synthesised in order to decrease the reaction times and to obtain crystals which are large enough to realise accurate electron microprobe analysis.

The determination of the SnO_2–ZrO_2 phase diagram is the first part of a more important research program which is devoted to the determination of the corrosion mechanisms of materials (ceramics and alloys) in silicate melts.[6,7] The knowledge of basic data will allow to choose the exact SnO_2–ZrO_2 ceramic compositions for required applications. The $(Sn_{1-x}Zr_x)O_2$ and $(Zr_{1-x}Sn_x)$ O_2 solid solutions are also studied by X-ray powder diffraction at room temperature and at $T=$ 1180 °C.

* Corresponding author.
E-mail address: renaud-podor@lcsm.uhp-nancy.fr (R. Podor).

0955-2219/02/$ - see front matter
PII: S0955-2219(02)00034-1

2. Experimental procedure

2.1. Starting materials

- ZrO_2 (Prolabo) containing 1.5 wt.% of HfO_2 (this content was determined by EPMA),
- CoO (Aldrich), 99.9% purity,
- SnO_2 (Chempur), 99 + % purity.

The starting powders were obtained by grinding of the exact quantities of each compound in an agate mortar. Syntheses of SnO_2 ceramics containing small amounts of ZrO_2 were performed by mechanical mixing using steel-alloy jars and balls for 30 min. The contamination of reactants by iron or iron oxides was not observed by EPMA nor X-ray diffraction.

The powders were granulated and the pellets were uniaxially pressed at 200 MPa to a green density of approximately 50% of the theoretical density.

The samples were sintered in a Gero furnace in the temperature range 1230–1750 °C. The samples were introduced and removed in the furnace at the desired temperature. The run duration time was decreased with increasing temperature, in order to limit the SnO volatilisation during high temperature experiments [according to Eq. (1)].

2.2. Analytical methods

The compositions of the different synthesised phases were determined by electron-probe microanalyses using a CAMECA SX50 electron microprobe equipped with four wavelength-dispersive spectrometers. The instrument operating conditions were 15 kV accelerating voltage, 10 nA probe current and 1 μm probe diameter. Counting times on standards and samples were determined in order to obtain a good accuracy for the element content analyses (operating conditions are summarised in Table 1). The oxygen contents were calculated by stoichiometry. Oxidation state for tin and zirconium is + IV; it is fixed at + II for cobalt. The error on the determination of weight per cent of Zr is ±0.30 for an initial weight content of 14.93. The experimental error on the determination of weight per cent of Sn is ±0.40 for a weight content of 12.02.

Powder X-ray measurements were performed by means of a PHILIPS X'Pert PRO diffractometer with a Cu(Kα) source ($\lambda = 1.54056$ Å) in the Bragg Brentano θ–θ geometry. The scans were carried out with a 0.01° step, a 2.5 seconds recording time for each position, over the range 15–100°. The $CuK_{\alpha 1}$ and $CuK_{\alpha 2}$ doublets were easily resolved using an automatic procedure of the DiffracAT program.[8]

The high-temperature X-ray diffractograms were recorded using a HTK 1200 temperature cell (Anton Parr) equipped with a Kanthal APM heater, Kapton-aluminium window foils and a sample spinner working at 30 rotations per minute. The temperature is limited to 1200 °C.

Determination of the unit-cell parameters. The lattice parameters were refined with the U-Fit program[9] with a 0.0005 Å precision on each parameter. The unit-cell parameters of the $(Zr_{1-x}Sn_x)O_2$ solid solution were refined in the monoclinic system (according to JCPDS card No. 37–1484; baddeleyte type),[10] from the data collected at room temperature. The unit-cell parameters of the $(Zr_{1-x}Sn_x)O_2$ solid solution were refined in the tetragonal system (according to JCPDS card No. 17–927),[11] from the data collected at $T = 1180$ °C.

Determination of the phase transition temperature—X-ray diffractograms were recorded in the region 27.5–32° 2θ in order to observe the $(11\overline{1})$ and (111) reflections of the monoclinic zirconia and the (111) reflection of the tetragonal zirconia. The high-temperature diffractograms were recorded each 10 °C step from 1080 °C to 1180 °C. The temperature was increased with a heating rate 2 °C min^{-1} and the samples were maintained at the desired temperature during 20 min before the recording of the diffractogram. A complete 2θ scan was carried out at 1180 °C for each sample in order to determine the cristallographic parameters of the tetragonal form of the $(Zr_{1-x}Sn_x)O_2$ solid solution. A series of diffractograms was recorded with decreasing temperature from 1180 to 800 °C with a 10 °C step in order to characterise the t→m transition with increasing SnO_2 content. The data obtained are correlated with DTG-DTA curves.

The relative amounts of monoclinic zirconia were estimated using the following formula, proposed by Garvie and Nicholson.[12]

Table 1
Operating conditions for electron microprobe analyses

Element	X-ray	Standard	Counting time on peak for standard (s)	Counting time on background for standard (s)	Counting time on peak for sample (s)	Counting time on background for sample (s)
Sn	Lα	SnO_2	30	2×30	15	2×15
Zr	Lα	ZrO_2	30	2×30	15	2×15
Hf	Mα	Hf	30	2×30	15	2×15
Co	Kα	Co	30	2×30	15	2×15

$$V_m = \left[I_m\left(11\bar{1}\right) + I_m(111)\right] / \left[I_m\left(11\bar{1}\right) + I_m(111) + I_t(111)\right] \quad (2)$$

$$V_t = 1 - V_m \quad (3)$$

where: V_m = volume fraction of the monoclinic zirconia, V_t = volume fraction of the tetragonal zirconia, $I_m(11\bar{1})$ = intensity of the $(11\bar{1})$ X-ray diffraction line for the monoclinic form of zirconia, $I_m(111)$ = intensity of the (111) X-ray diffraction line for the monoclinic form of zirconia, $I_t(111)$ = intensity of the (111) X-ray diffraction line for the tetragonal form of zirconia.

DTA-DTG measurements were performed using a Setaram TG92–16. For each sample, the experiments were carried out using an identical processing route. Each ceramic (100 mg) was introduced in an alumina nacelle. The sample was heated to 800 °C with a heating rate of 10 °C min^{-1}, heated to 1400 °C with a heating rate of 2 °C min^{-1}, cooled to 800 °C with a cooling rate of 2 °C min^{-1} and cooled to room temperature with a cooling rate of 10 °C min^{-1}.

3. Results and discussion

3.1. SnO_2–ZrO_2 phase diagram

First attempts to determine the SnO_2–ZrO_2 phase diagram have been carried out earlier.[13,14] Equimolar mixtures of pure SnO_2 and ZrO_2 were prepared in order to study the SnO_2–ZrO_2 phase diagram in the temperature range 1230–1750 °C. One reverse run was carried

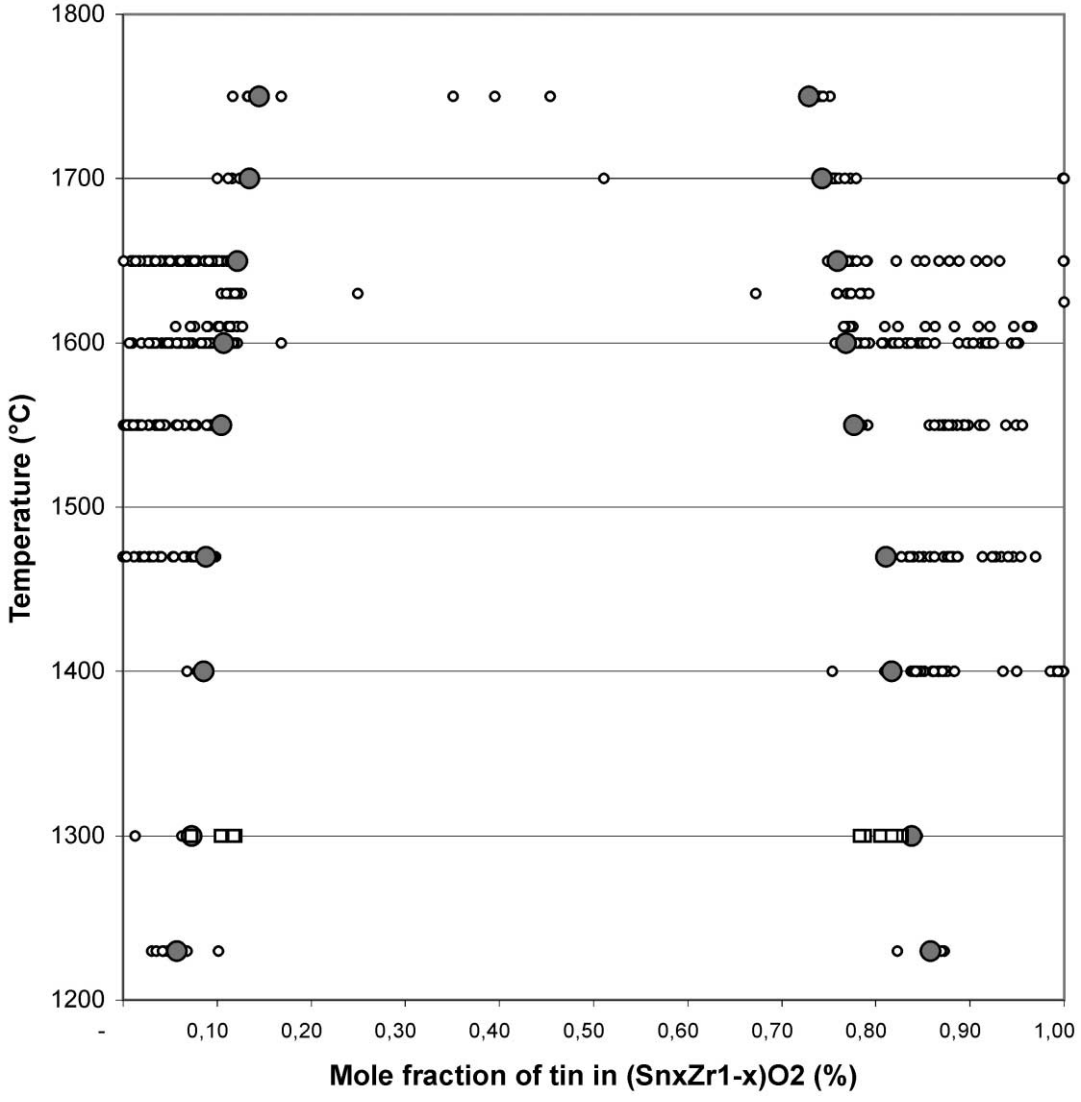

Fig. 1. Phase diagram between ZrO_2 and SnO_2 in the 1200–1750 °C temperature range. The solvus was determined using a mechanical mixture of pure SnO_2 and ZrO_2 phases (open circles) or a supersaturated mixture (open squares). The filled circles represent the estimated equilibrium compositions.

out by heating at $T=1300$ °C a two-phased sample previously annealed at $T=1600$ °C and quenched in air. The experimental results are summarised in Fig. 1, in the form of a phase-diagram. Fig. 2 shows a microphotograph of an equimolar mixture of SnO_2 and ZrO_2 equilibrated at 1300 °C. The equilibrium between both SnO_2 Zr-rich and ZrO_2 Sn-rich phases was reached after a 48 h long run at this temperature. Wilson and Glasser[13] and Kim et al.[14] have reported data concerning the equilibrium between SnO_2 and ZrO_2 at $T=1550$ °C and $T=1500$ °C respectively. Wilson and Glasser[13] have determined that 10% of SnO_2 can be incorporated into zirconia, and that this phase is in equilibrium with SnO_2 containing 18% of ZrO_2. These results were obtained from electron microprobe analyses. Kim et al.[14] have determined from X-ray data and Raman spectroscopy that the solubility limit of tin oxide into zirconia is equal to 8 wt.% at $T=1500$ °C. An immiscibility gap occurs between both phases in the temperature range which was explored, leading to two limited solid solutions of zirconia into SnO_2 and of SnO_2 into zirconia. The solubility of one in each other slowly increases with increasing temperature. It was impossible to determined if ZrO_2 and SnO_2 form a complete solid solution at a higher temperature by the experimental procedure. Attempts to achieve experiments at temperature above 1750 °C using an experimental gas furnace all yielded to the complete volatilisation of SnO_2. Indeed, an increase of the SnO_2 decomposition into SnO and O_2 was observed when increasing temperature. The substitution of Zr in the SnO_2 lattice is not sufficient to stabilise the compound at high temperature.

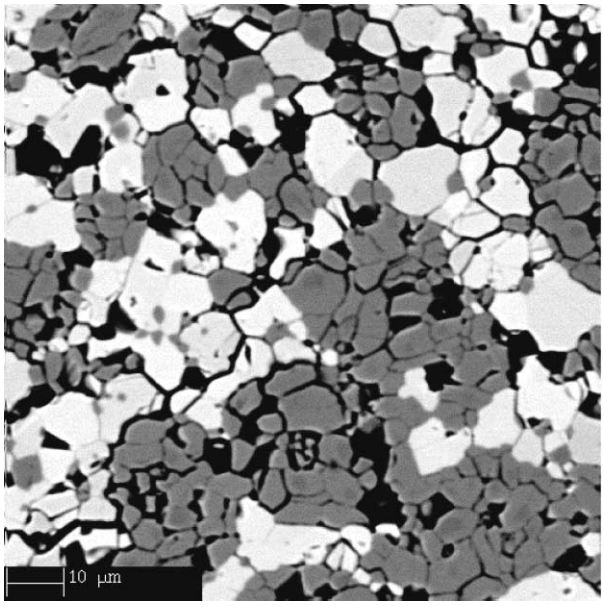

Fig. 2. Microphotograph of an equimolar mixture of SnO_2 and ZrO_2 equilibrated at 1130 °C (white grains correspond to SnO_2-rich phase and dark-grey grains correspond to ZrO_2-rich phase).

3.2. Crystallographic data

Pure phases were prepared in order to study both ZrO_2 and SnO_2-rich solid solutions by X-ray powder diffraction.

3.2.1. $(Sn_{1-x}Zr_x)O_2$ solid solution

The annealing procedure gave good $(Sn_{1-x}Zr_x)O_2$ single-phase ceramics, as determined by electron microprobe analyses. The determination of the unit-cell parameters of pure SnO_2 and the unit-cell parameters of 0.5 mol% CoO-doped SnO_2 yields to the same set of values. The incorporation of small amounts of CoO in the matrix does not modify significantly the structure of the compounds which were prepared.

The parameters determined for the single-phase $(Sn_{1-x}Zr_x)O_2$ compounds are plotted in Fig. 3 as a function of the ZrO_2 mole fraction. All the data (a, c and the cubic root of the unit-cell volume) can be fitted by a linear curve. In this domain of compositions, no deviation from Vegard's law has been observed, on the contrary of what has been shown in the SnO_2–TiO_2 system.[15] The increase of the unit-cell parameters with increasing ZrO_2 mole fraction is due to the substitution of Sn^{4+} (which ionic radius is 0.69 Å in the sixfold coordination)[16] by Zr^{4+} (which ionic radius is 0.72 Å in the sixfold coordination).

3.2.2. $(Zr_{1-x}Sn_x)O_2$ solid solution

Zirconia doped with SnO_2 is not stabilised in the tetragonal structure at room temperature, and the compounds obtained are crystallised in the monoclinic structure when quenched at room temperature. Nevertheless, Wilson and Glasser[13] have shown that SnO_2-rich zirconia is tetragonal at high temperature. In this study, no oxide (CaO, MgO or Y_2O_3) has been added to

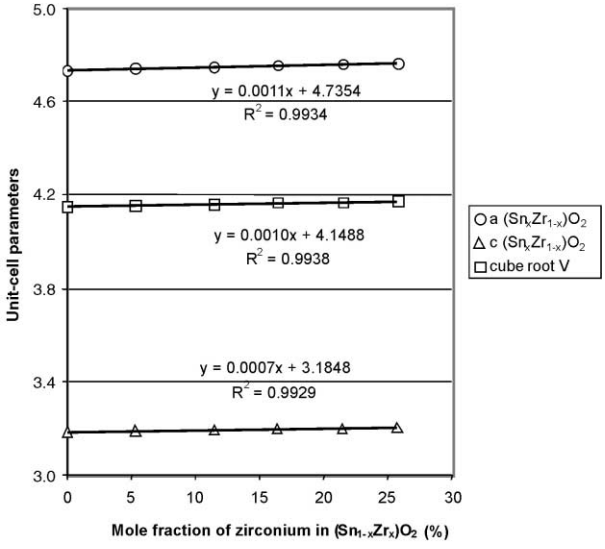

Fig. 3. Unit-cell parameters for the $(Sn_{1-y}Zr_y)O_2$ solid solution.

stabilise the tetragonal form. Products with general compositions $(Zr_{1-x}Sn_x)O_2$ were prepared with maximum SnO_2 mole fraction equal to 13.8%. X-ray diffractograms were recorded at room temperature and at $T = 1180$ °C, in order to determine the unit-cell parameters of the $(Zr_{1-x}Sn_x)O_2$ solid solution in both monoclinic (low-temperature form) and tetragonal (high-temperature form) systems. The lattice parameters which were determined from these measurements are summarised in Table 2.

No data are available in the literature concerning the monoclinic form of zirconia doped with tin oxide. The unit-cell parameters which are determined in this work are reported versus the mole fraction of tin incorporated in ZrO_2 in Fig. 4a. In the domain of stability of the $(Zr_{1-x}Sn_x)O_2$ solid solution, no deviation from the Vegard's law is observed. Nevertheless, the insertion of tin in the baddeleyte lattice involves a distortion of the unit-cell. The *a*-parameter increases with increasing tin content in the lattice whereas *b*, *c* and β decrease when increasing SnO_2 mole fraction in the material. The volume of the unit-cell does not depend on the tin content. That is to say that the incorporation of tin in monoclinic ZrO_2 yields to a distortion of the unit-cell which corresponds to a compression along the b and c axis and a dilatation along the a axis.

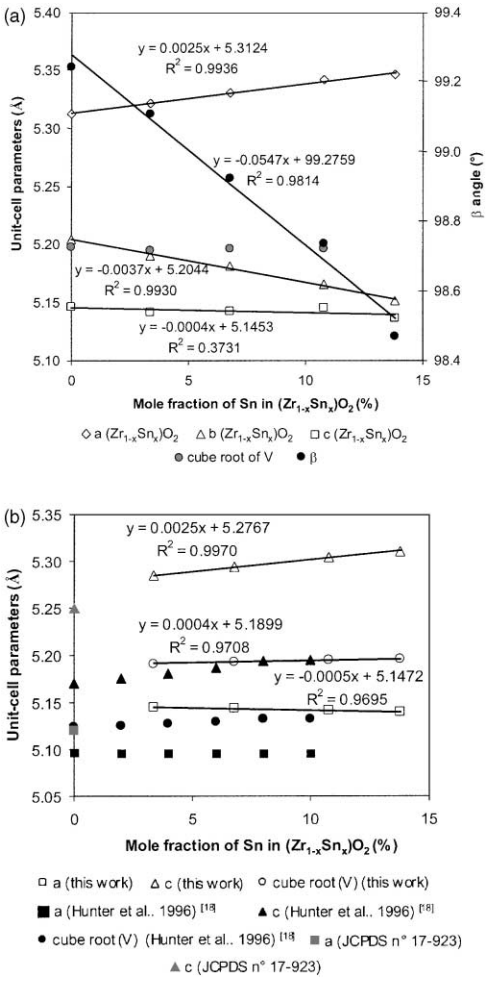

Fig. 4. Unit-cell parameters for the $(Zr_{1-x}Sn_x)O_2$ solid solution. (a) Monoclinic system (X-ray diffractograms were recorded at 25 °C). (b) Tetragonal system (X-ray diffractograms were recorded at 1180 °C for data determined in this work).

The unit-cell parameters of the tetragonal form of the $(Zr_{1-x}Sn_x)O_2$ solid solution were determined from high-temperature X-ray diffractograms recorded at 1180 °C. They are plotted versus the tin oxide content in Fig. 4b. These results are compared with those determined by Kim et al.[14] and Hunter et al.[17] for the $(Zr_{0.98-x}Y_{0.02}Sn_x)O_2$ series. These authors have studied the yttria-stabilized zirconia with tin. In their study, the unit-cell parameters were determined at room temperature from neutron diffraction measurements. The set of data obtained in this work[17] indicates that the unit-cell volume of tetragonal $(Zr_{1-x}Sn_x)O_2$ solid solution is lowered by the incorporation of yttria used to stabilise the tetragonal zirconia. The same variations of the unit cell parameters when increasing tin oxide in ZrO_2 and $Zr_{0.98}Y_{0.02}O_2$ are observed in both works.

3.3. Physico-chemical properties

The monoclinic to tetragonal (noted m→t) and reverse tetragonal to monoclinic (noted t→m) temperature transitions were characterised by high-temperature X-ray diffraction and DTG-DTA measurements for each composition of the $(Zr_{1-x}Sn_x)O_2$ solid solution, as described in the experimental method section. It is to be noted that $(Zr_{0.93}Sn_{0.07})O_2$, $(Zr_{0.89}Sn_{0.11})O_2$ and $(Zr_{0.86}Sn_{0.14})O_2$ compounds are metastable phases when *T* is lower than 1180 °C.

The volume fractions of monoclinic and tetragonal $(Zr_{0.89}Sn_{0.11})O_2$ zirconia for the heating and cooling experiments are reported in Fig. 5a. The highest temperature which has been explored by this method is 1180 °C. At the higher heating temperature, the monoclinic to tetragonal phase transformation is never complete, and almost 10% of monoclinic zirconia still be stable at this temperature. This may be due to the grain size of the specimens (which is not taken into account in this study) which should be considered in the evaluation of a more precise effect of the dopant. The decreasing temperature experiments have been performed by cooling of the products obtained after heating at the maximum temperature. In this case, the volume fraction of the tetragonal zirconia stabilised at high temperature is the only part of the product which can be transformed into monoclinic zirconia by decreasing the temperature and it can be considered as 100% of the product which can be transformed by cooling. The volume fractions of monoclinic zirconia obtained by the transformation of tetragonal zirconia during cooling are derived from this initial part of tetragonal zirconia. From these data, the

Table 2
Unit-cell parameters for $(Sn_{1-x}Zr_x)O_2$ and $(Zr_{1-x}Sn_x)O_2$ solid solutions

x_{Zr}	a (Å)	Δa (Å)	c (Å)	Δc (Å)					R (%)
$(Sn_{1-x}Zr_x)O_2$ solid solution									
0	4.7352	0.0003	3.1844	0.0004					1.7
5.34	4.7418	0.0006	3.1890	0.0007					2.6
11.49	4.7479	0.0006	3.1922	0.0008					3.1
16.41	4.75478	0.0006	3.19664	0.0008					2.8
21.48	4.7581	0.0006	3.19873	0.00069					2.4
25.77	4.76519	0.0005	3.20233	0.00069					3.8
X_{Sn}	a (Å)	Δa (Å)	b (Å)	Δb (Å)	c (Å)	Δc (Å)	β (°)	$\Delta\beta$	R (%)
$(Zr_{1-x}Sn_x)O_2$ solid solution									
Low-temperature form									
0	5.312	0.0006	5.2042	0.0005	5.1462	0.0007	99.243	0.012	1.47
3.36	5.3207	0.0012	5.1903	0.0012	5.1416	0.0011	99.108	0.018	2.36
6.78	5.3295	0.0011	5.1817	0.001	5.1423	0.0011	98.925	0.019	2.10
10.77	5.3408	0.0012	5.1653	0.0012	5.1454	0.0009	98.737	0.017	2.03
13.8	5.3453	0.0034	5.1516	0.0040	5.1368	0.0027	98.469	0.052	2.72
x_{Zr}	a (Å)	Δa (Å)	c (Å)	Δc (Å)					R (%)
High-temperature form									
3.36	5.1449	0.0004	5.2847	0.0005					0.7
6.78	5.144	0.0003	5.2937	0.0003					0.4
10.77	5.1414	0.0004	5.3042	0.0004					0.6
13.8	5.1393	0.0013	5.3103	0.0014					1.7

relative temperatures corresponding to the beginning of the m→t and reverse transitions can be determined (as well as the temperatures corresponding to the half m→t and reverse reaction) were determined from X-ray diffraction data (Fig. 5a) and reported in Fig. 5b. The corresponding phase transition temperatures were determined from DTG-DTA measurements. They are also reported in Fig. 5b. Both set of data indicates clearly that the incorporation of SnO_2 into zirconia involves the decrease of the phase transition temperatures. The tetragonal form of zirconia is stabilised when incorporating SnO_2 into the matrix. One can note that the hysteresis effect observed on pure zirconia is also exhibited in this study.

These results are in good agreement with those reported by Wilson and Glasser[13] and Kim et al.,[14] who have shown that tetragonal zirconia solid solutions with SnO_2 cannot be retained at room temperature because the t→m phase transition is not depressed enough by adding SnO_2. Nevertheless, these authors have reported that the m→t phase transformation temperature of zirconia solid solutions is decreased by adding SnO_2 as dopant.

The tetragonality parameter (c/a axial ratio) is considered to be a parameter which reflects the stabilisation of the tetragonal form of zirconia. Li et al.[18] suggested that the stability of t-zirconia that have been doped with undersized tetravalent cations (cations smaller than Zr^{4+}) increases with tetragonality, because the rise of tetragonality is equivalent to the decrease in strain

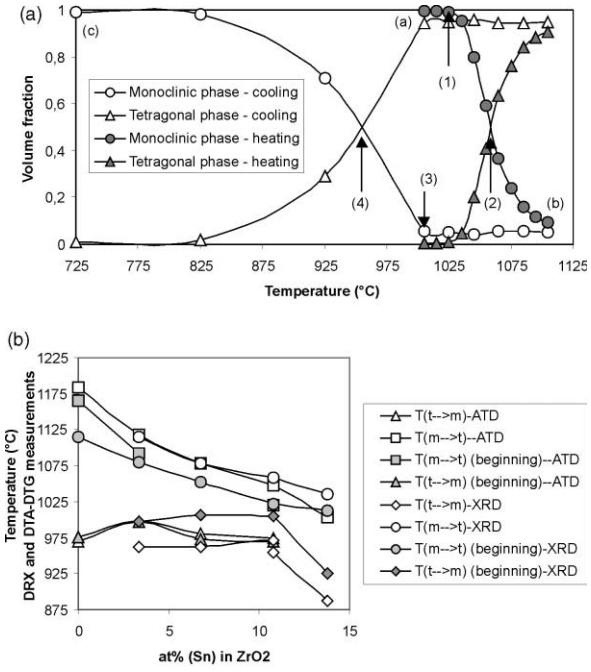

Fig. 5. (a) Volume fraction of the monoclinic and tetragonal zirconia [$(Zr_{0.89}Sn_{0.11})O_2$ composition] represented as a function of temperature. The heating of the product goes from (a) to (b), and the cooling of the compound goes from (b) to (c). Point (1) corresponds to the (m→t) beginning phase transition, point (2) corresponds to the (m→t) half phase transition, point (3) corresponds to the (t→m) beginning phase transition, point (4) corresponds to the (t→m) half phase transition. (b) Temperatures of (m→t) and (t→m) phase transformations, obtained from X-ray diffraction and DTA-DTG data.

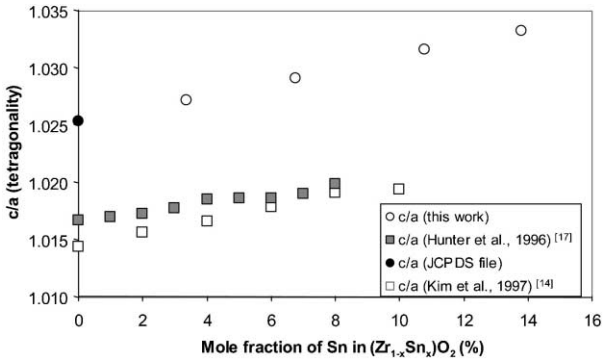

Fig. 6. c/a Axial ratio (tetragonality) reported as a function of mole fraction of tin in the tetragonal zirconia for the $(Zr_{1-x}Sn_x)O_2$ series (this work and JCPDS card n° 17–927) and for the $(Zr_{0.98-x}Y_{0.02}Sn_x)O_2$ series.[14,17].

energy in the tetragonal zirconia lattice, as a result of cation ordering. The c/a axial ratios calculated from the unit-cell parameters determined in this work and from data collected in the literature[14,17] are reported in Fig. 6 as a function of the mole fraction of tin oxide incorporated in zirconia. It appears clearly that tetragonality increases with increasing dopant content, and that this parameter is correlated with the decrease of the m→t (and t→m) phase transformation temperature in the $(Zr_{1-x}Sn_x)O_2$ solid solution. The c/a axial ratios calculated for the $(Zr_{0.98-x}Y_{0.02}Sn_x)O_2$ solid solution are lowered in comparison with those calculated for the $(Zr_{1-x}Sn_x)O_2$ series, but slowly increase with increasing tin content.

4. Conclusions

It is now clearly proven that only limited solid solutions exist in the $(Sn_{1-x}Zr_x)O_2$ and $(Zr_{1-x}Sn_x)O_2$ systems in the 1230–1750 °C temperature range. The $(Sn_{1-x}Zr_x)O_2$ phases can be obtained with a density close to the theoretical density by adding 0.5 mol% of CoO. From the results obtained in this study, new ceramic-based materials will be elaborated in the form of small crucibles to study their stability against silicate melts.

Acknowledgements

The authors gratefully acknowledge S. Barda and F. Diot (Service Commun d'Analyses par Sondes Electroniques—Nancy), J.P. Emeraux and L. Aranda (Laboratoire de Chimie du Solide Minéral—Nancy) and A. Rouillet (Centre de Recherches Pétrographiques et Géochimiques—Nancy) for their helpful assistance.

References

1. Hoenig, C. L. and Searcy, A. W., Knudsen and Langmuir evaporation studies of stannic oxide. *J. Am. Ceram. Soc.*, 1966, **49**, 128–134.
2. Leite, E. R., Cerri, J. A., Longo, E., Varela, J. A. and Paskocima, C. A., Sintering of ultrafine undoped SnO2 powder. *J. Eur. Ceram. Soc.*, 2001, **21**, 669–675.
3. Cerri, J. A., Leite, E. R., Gouvea, D., Longo, E. and Varela, J. A., Effect of cobalt (II) oxide and manganese (IV) oxide on sintering of tin (IV) oxide. *J. Am. Ceram. Soc.*, 1997, **79**(3), 799–804.
4. Bonnet, J. P., Dolet, N. and Heintz, J. M., Low temperature sintering of 0.99 SnO2–0.01 CuO: influence of copper surface diffusion. *J. Eur. Ceram. Soc.*, 1996, **16**, 1163–1169.
5. Lalande, J., Ollitraut-Fichet, R. and Boch, P., Sintering behaviour of Cuo-doped SnO_2. *J. Eur. Ceram. Soc.*, 2000, **20**, 2415–2420.
6. Lizarazu, D., Steinmetz, P. and Bernard, J. L., Corrosion of nickel-chromium alloys by molten glass at 1100 °C; an electrochemical study. *Materials Science Forum*, 1997, **251–254**(Part 2), 709–720.
7. Kessler, O., *Alliages Réfractaires Résistants à la Corrosion par le verre Fondu: Synthèse et Caractérisation*. PhD thesis, Université Henri Poincaré, Nancy, France, 1997 (in French).
8. Caussin, P., Nisinovici, J. and Beard, D. W., Diffract-AT program. *Adv. X-Ray Analy.*, 1988, **31**, 423.
9. Evain, M., *U-fit Program*. Institut des Matériaux de Nantes, France, 1992.
10. McMurdie, H., Morris, M., Evans, E., Wong-Ng, W. and Bttinger, L., *Powder Diffr.*, 1986, **1**, 76.
11. JCPDS Card No. 17–927; US Bureau of Mines—open file report.
12. Garvie, R. C. and Nicholson, P. S., Phase analysis in zirconia systems. *J. Am. Ceram. Soc.*, 1972, **55**, 303–305.
13. Wilson, G. and Glasser, F. P., Solid solutions in the ZrO_2–SnO_2–TiO_2 system. *Br. Ceram. Trans. J.*, 1989, **88**(33), 69–74.
14. Kim, D. J., Jang, J. W. and Lee, H. L., Effect of tetravalent dopants on raman spectra of tetragonal zirconia. *J. Am. Ceram. Soc.*, 1997, **80**(6), 1453–1461.
15. Park, M., Mitchell, T. E. and Heuer, A. H., Subsolidus equilibriums in the titanium (IV) oxide–tin(IV) oxide system. *J. Am. Ceram. Soc.*, 1975, **58**(1–2), 43–47.
16. Shannon, R. D., Revised effective ionic radii and systematic studies of interatomic distances in halides and chalcogenides. *Acta Cristallographica*, 1976, **A32**, 751–767.
17. Hunter, B. A., Howard, C. J. and Kim, D. J. Neutron diffraction study of tetragonal zirconias containing Sn. *Physica B*, 1998, 41–243, 1249–1251.
18. Li, P., Chen, I. W. and Penner-Hahn, J. E., The effects of dopant on zirconia stabilization—an X-ray absoption study: II—tetravalent dopants. *J. Am. Ceram. Soc.*, 1994, **77**(5), 1281–1288.